Characterization of phase-transition-induced micro-domain structures in vanadium dioxide

Ping Lu[a,b,c], Jiadong Zhou[c,d], Xinling Liu[d,e], Zongtao Zhang[d,f], Fangfang Xu[*,a,b], Linlin Zhang[a, b], Xinliang Mou[a,b,c], Jingwei Feng [a,b], Yanfeng Gao[d,e], Jingtai Zhao[g]

[a] State Key Laboratory of High Performance Ceramics and Superfine Microstructures, and
[b] Analysis and Testing Center for Inorganic Materials, Shanghai Institute of Ceramics, Chinese Academy of Science (CAS), 1295 Dingxi Road, Shanghai 200050, China
[c] University of Chinese Academy of Sciences, 19 Yuquan Road, Beijing 100049, China
[d] Ancient Ceramics Research Center, Shanghai Institute of Ceramics, Chinese Academy of Science (CAS), 1295 Dingxi Road, Shanghai 200050, China
[e] School of Materials Science and Engineering, Shanghai University, 99 Shangda Road, Shanghai 200444, China
[f] School of Materials Science and Engineering, Zhengzhou University, Zhengzhou, 450001, China
[g] Artificial Crystal Research Center, Shanghai Institute of Ceramics, Chinese Academy of Science (CAS), 1295 Dingxi Road, Shanghai 200050, China

The detailed crystallography parameters of different phases of VO_2 are listed in Table S1. The data are searched from the Landolt-Bornstein database.

Table S1. Crystallography parameters of different phases of VO_2

Phase	LPF ID number	Space group	Crystallography parameters					
			a(nm)	b(nm)	c(nm)	α(°)	β(°)	γ(°)
R	SD308884	$P4_2/mnm(136)$	0.4552	0.4552	0.2851	90	90	90
M1	SD455502	$P2_1/c(14)$	0.53591	0.4525	0.5386	90	115.232	90
M2	SD1905614	C2/m(12)	0.9083	0.5763	0.4523	90	90.3	90

The subgroup chains (Fig. S1) used for the decomposition of the space group of the parent phase R show the symmetry correlations between the low temperature phase (M1 or M2) and the high temperature phase (R). It can be seen that the $2_1/c$ in M1 phase originates from the $2_1/n$ along $\mathbf{b_R}$, while the 2/m in M2 phase originates from 2/m along $\mathbf{c_R}$. Both M1 and M2 lose the translation of $\mathbf{c_R}$. The transformation relationships between them are also represented in Fig. S1.

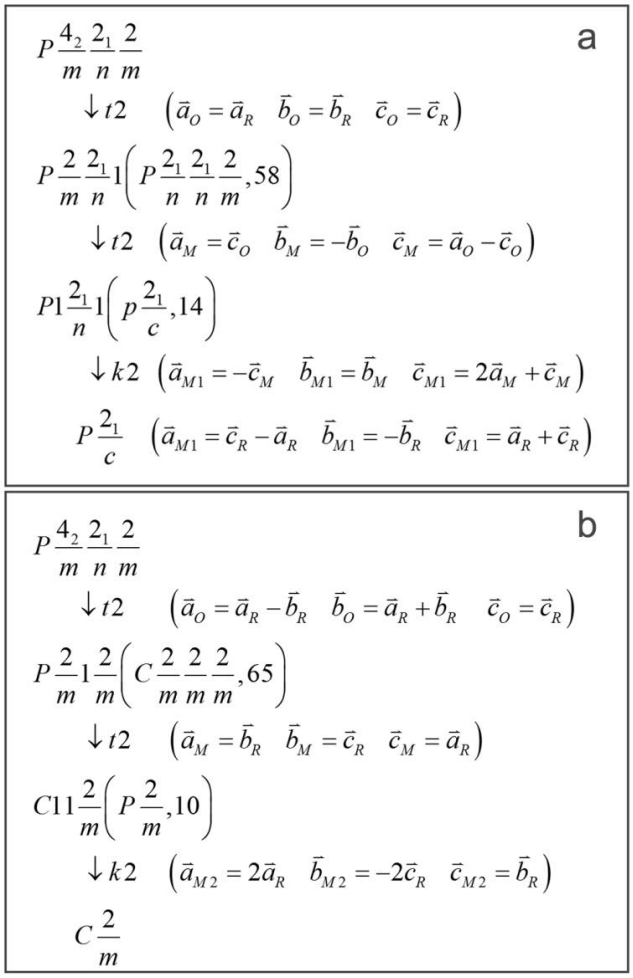

Figure S1. Chain of Subgroups and transformation relationships: (a) Derivation chain of the subgroups of M1 from R; (b) Derivation chain of the subgroups of M2 from R.

The formation of $2[110]_{M1}$ twins is shown in Fig. S2. The vanadium atoms shown as cycles (of M1) and stars (of $M1_T$) are projected along $\mathbf{c_R}$. The vanadium atoms in M1 or $M1_T$ pair along $\mathbf{c_R}$ and twist perpendicular to $\mathbf{c_R}$. The twisting ways in M1 and $M1_T$ are different but are connected by the 180° rotation along $[110]_R$. Since the $2[110]_R$ are one of the symmetry operations in R phase, the two ways of twisting are equivalent from R to M1. Cells of M1 and $M1_T$ are defined as blue and red dotted lines, respectively.

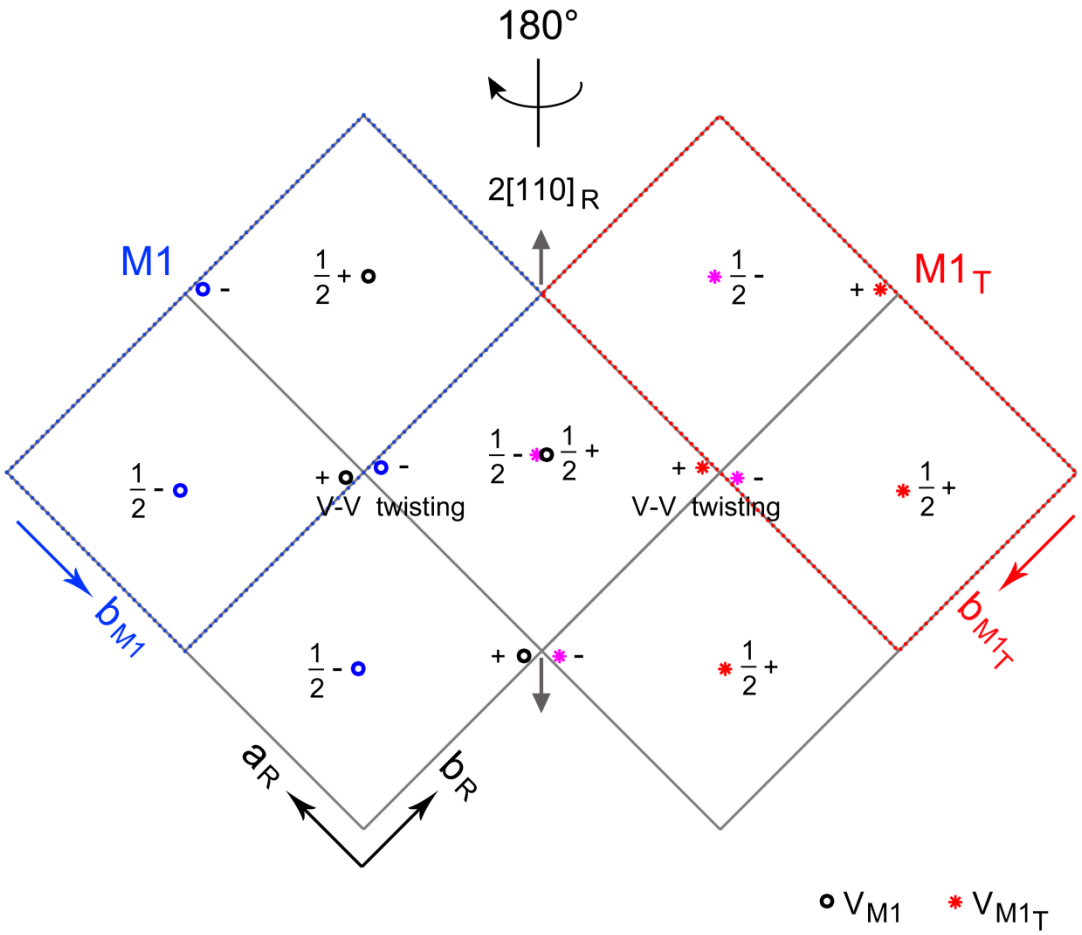

Figure S2. The formation of 2[110]R twins in M1 phase:

The High resolution TEM image (Fig. S3a) of the particle in the powder sample (shown in Fig. 3a) reveals antiphase boundaries (APBs) as arrowed. The IFFT images with the reflections of ±002 and $\pm\bar{2}02$ (Fig. S3c and S3d) show no displacement at the APBs. The dot product of the displacement between the antiphase domains and the hkl plane ($\mathbf{D_{shift} \cdot g_{hkl}}$) must be integral, which matches the theoretical analysis ($\mathbf{D_{shift}}=1/2[1\ 0\ 1]_{M1}$).

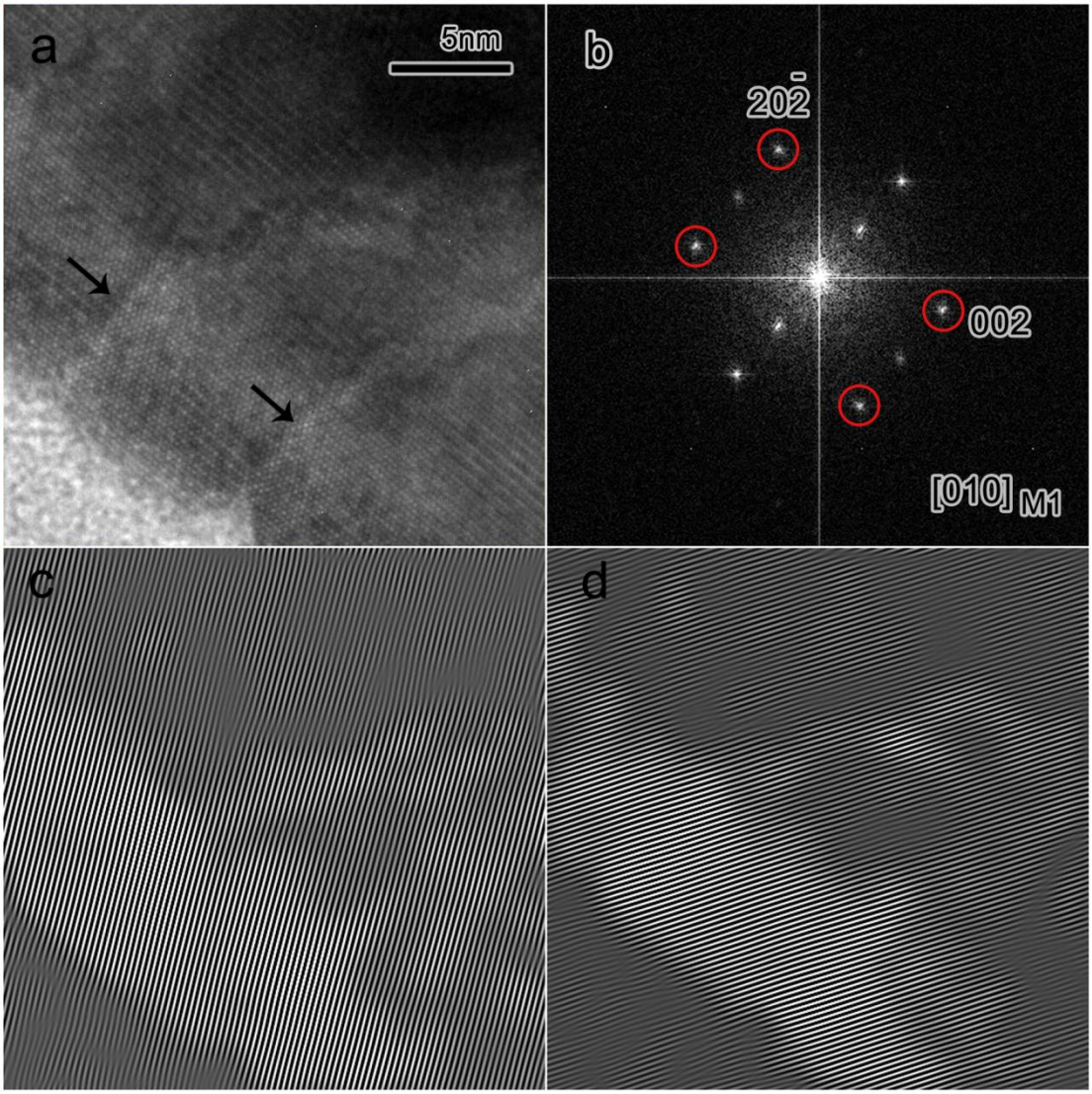

Figure S3. Characterization of antiphase domains: (a) High resolution TEM image of the particle in the powder sample, on which the antiphase boundaries (APBs) are arrowed. (b) Fast Fourier transform (FFT) of (a). (c) and (d) are the Inverse FFT image with the reflections of 002 and $\bar{2}02$, respectively. The IFFT images show no displacement at the APBs.

Due to the similarity of the diffraction patterns of M1 and M2, the diffraction pattern shown in Fig. 1b can also be indexed as M2 twin structures. By comparing the experimental diffraction pattern to the simulative ones of different twin domains along the same zone axis, the domain structures shown in Fig. 1a can also be identified as the $2[110]_R$ (or $2[102]_{M2}$) twin domains or the 4_2^+ $[001]_R$ (or $4_1^+[0\text{-}10]_{M2}$) translation-twin domains of M2 phase. Detailed indexation is shown in Fig. S4.

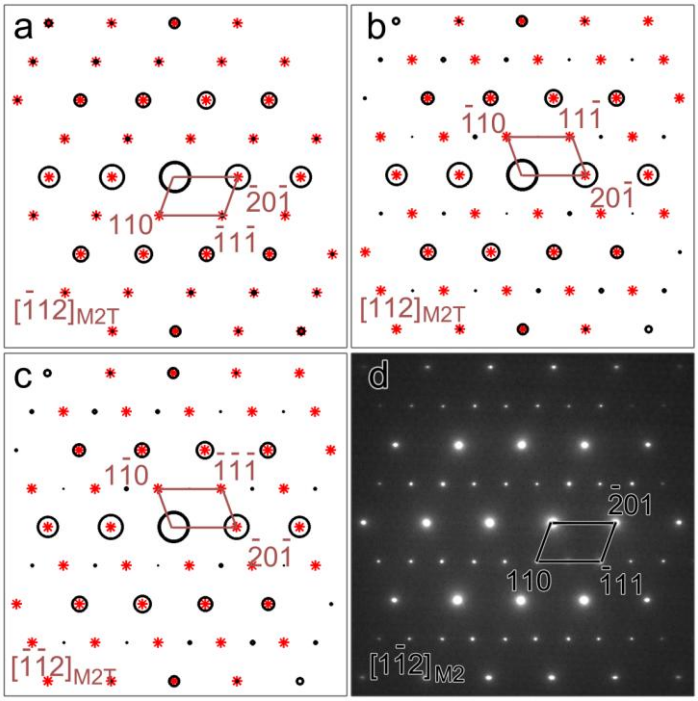

Figure S4. Indexation of diffraction pattern of M2 domains: (a) Simulative diffraction pattern of $n[010]_R$ translation-twin domains; (b) Simulative diffraction pattern of $2[110]_R$ rotation twin domains; (c) Simulative diffraction pattern of 4_2^+ $[001]_R$ translation-twin domains; (d) Experimental diffraction pattern of domain structure in Fig. 1a.

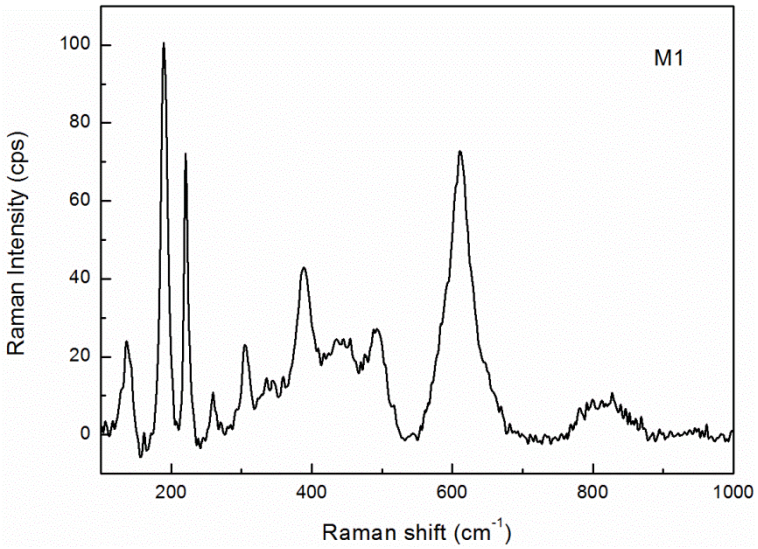

Figure S5. Raman spectrum of the film sample at room temperature, which matches well with the spectrum of M1 phase of VO_2 while no M2 phase is detected.

Raman measurements are performed at the DXR Raman microscope (Thermo Nicolet, USA). The sample was excited by the 532nm laser. Raman spectrum of the film sample is shown in Fig. S5, which matches well with the spectrum of M1 phase of VO_2 reported by other groups (Zhang et al., 2011; Strelcov et al., 2012).

Reference

Strelcov, E., Tselev, A., Ivanov, I., Budai, J. D., Zhang, J., Tischler, J. Z., Kravchenko, I., Kalinin, S. V, & Kolmakov, A. (2012). *Nano Lett.* **12**, 6198–6205.

Zhang, S., Kim, I. S., & Lauhon, L. J. (2011). *Nano Lett.* **11**, 1443–1447.